energies

MDPI

Article

The Heat-Storing Micro Gas Turbine—Process Analysis and Experimental Investigation of Effects on Combustion

Eleni Agelidou [1], Hannah Seliger-Ost [1,*], Martin Henke [1], Volker Dreißigacker [2], Thomas Krummrein [1] and Peter Kutne [1]

[1] Institute of Combustion Technology, German Aerospace Center, Pfaffenwaldring 38-40, 70569 Stuttgart, Germany
[2] Institute of Engineering Thermodynamics, German Aerospace Center, Pfaffenwaldring 38-40, 70569 Stuttgart, Germany
* Correspondence: hannah.seliger@dlr.de

Abstract: Renewable energy sources such as wind turbines and photovoltaics are the key to an environmentally friendly energy supply. However, their volatile power output is challenging in regard to supply security. Therefore, flexible energy systems with storage capabilities are crucial for the expansion of renewable energy sources since they allow storing off-demand produced power and reconverting and supplying it on-demand. For this purpose, a novel power plant concept is presented where high-temperature energy storage (HTES) is integrated between the recuperator and the combustor of a conventional micro gas turbine (MGT). It is used to store renewable energy in times of oversupply, which is later used to reduce fuel demand during MGT operation. Hereby, pollutant emissions are reduced significantly, while the power grid is stabilized. This paper presents a numerical process simulation study, aiming to examine the influence of different storage temperatures and load profiles of HTES on the MGT performance (e.g., fuel consumption, efficiency). Furthermore, relevant operating points and their process parameters such as pressures, temperatures, and mass-flow rates are derived. As operation conditions for the combustor are strongly influenced by the HTES, the paper contains a detailed theoretical analysis of the impact on combustor operability and includes an experimental investigation of the first combustor design adapted for the compound and tested under higher inlet temperatures conditions.

Keywords: micro gas turbine; MGT; HTES; high-temperature heat storage; FLOX®; jet-stabilized; combustor

Citation: Agelidou, E.; Seliger-Ost, H.; Henke, M.; Dreißigacker, V.; Krummrein, T.; Kutne, P. The Heat-Storing Micro Gas Turbine—Process Analysis and Experimental Investigation of Effects on Combustion. *Energies* **2022**, *15*, 6289. https://doi.org/10.3390/en15176289

Academic Editor: Andrzej Teodorczyk

Received: 1 July 2022
Accepted: 17 August 2022
Published: 29 August 2022

1. Introduction

1.1. Motivation and Concept

Providing sustainable energy is widely viewed as one of the biggest challenges in our modern society. One of the proposed pathways for climate change mitigation apart from efficient use of energy is to increase the use of renewable energy sources [1]. However, the enormous volatility associated with most renewable energy sources leads to grid instabilities and threatens supply reliability [2].

Decentralized combined heat and power units (CHP) can be utilized to counteract grid instabilities caused by a sudden loss of renewable energy generation due to their highly flexible power production capacities [2]. Besides the electrical power, decentralized CHP units also provide residual heat for downstream processes or residential heating [3]. With cogeneration, high overall efficiencies above 90% are achievable while transformer and transfer losses are avoided due to the proximity to the consumer [4]. Thus, this leads to a reduction in primary energy consumption and greenhouse gas emissions. Compared to common CHP technologies such as piston engines, MGT-based CHP systems are particularly suitable due to their high fuel flexibility along with low pollutant emissions [5], as well as their low maintenance costs, low noise emissions [6], and high load flexibility.

However, providing additional power production capacities alone will not enable the major expansion of renewable energies, as the grid cannot support the temporary overproduction of electrical energy inevitably associated with it.

To overcome these challenges, heat storages with high specific heat capacity are a promising solution since it can be easily scaled in size and enable temperatures above 1000 K [7]. When considering combining an HTES and an MGT another significant advantage of MGTs comes into play: HTES can be simply integrated into the MGT cycle and counteract grid instabilities caused by an overproduction of renewable energy. To use this potential, the HTES is integrated between the recuperator and the combustor of the MGT as shown in Figure 1 on the right side.

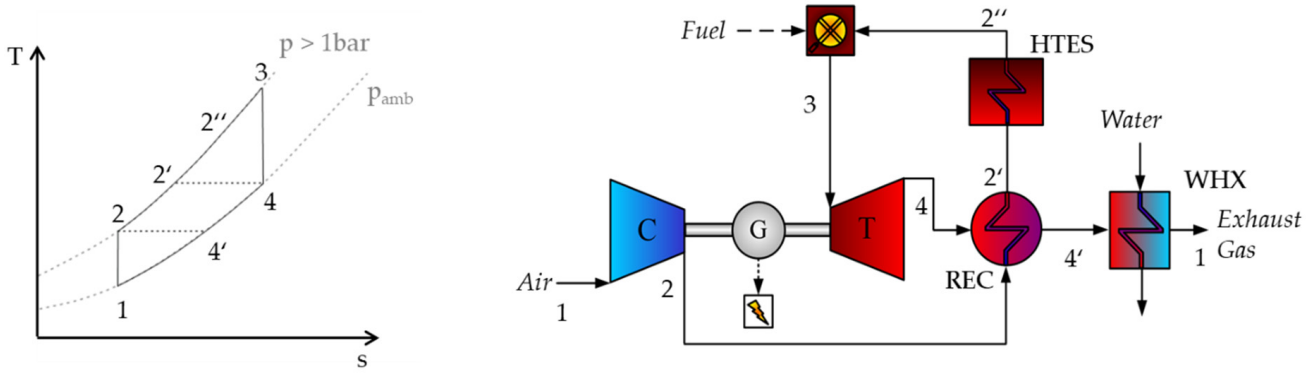

Figure 1. (**Left**): temperature-entropy diagram of an ideal Brayton cycle with an HTES. (**Right**): scheme of an MGT-based power plant coupled with an HTES.

The thermodynamic process of the MGT is described by the ideal recuperated Brayton Cycle. The temperature entropy diagram is illustrated in Figure 1 (right side). First, the air is compressed (isentropic compression $1 \rightarrow 2$), then preheated in the recuperator (isobaric heat addition $2 \rightarrow 2'$) and sent to the combustor. To reach the desired turbine inlet temperature (TIT) fuel is injected. After the combustion (isobaric heat addition $2' \rightarrow 3$) the hot exhaust gas is expanded by the turbine to atmospheric pressure (isentropic expansion $3 \rightarrow 4$). Downstream, in the recuperator, heat is transferred from the exhaust gas to the pressurized combustion air (isobaric heat rejection, $4 \rightarrow 4'$), reducing the fuel demand and therefore increasing the electrical efficiency of the system. In CHP applications residual thermal energy of the exhaust gas is used, e.g., as process heat or for residential heating. Hence, the exhaust gas temperature is further decreased in the water heat exchanger (WHX). When integrating an HTES the hot compressed air after the recuperator is further heated ($2' \rightarrow 2''$), increasing the combustion inlet temperature and allowing to dramatically reduce fuel consumption. Hence, higher power plant efficiencies and lower pollutant emissions are realized.

The advantage of the presented combination of an MGT with an HTES is that it enables the storage of renewable electrical power as heat when renewable energy sources surpass demand and electricity prices are low. This power is then reconverted and supplied according to the electrical and thermal demand, achieving both ecological and economic benefits.

Ideally, the HTES outlet temperature matches the combustor outlet temperature of a conventional MGT (>1000 K), so no fuel is necessary. However, also, the temperature profile itself has an impact on the CHP performance. High HTES temperatures can be achieved using solid media storage (see Section 1.2 below). When operating the compound and discharging the HTES the outlet temperature of the HTES decreases leading to a drop in the power output. To ensure a constant power output of the MGT, the combustor needs to compensate for the temperature drop. This leads to challenging combustor operation conditions namely very high inlet temperatures and very low fuel flow rates while having to ensure low emissions at the same time. Additionally, a low flashback risk

is required to enable (at least technically) premixed combustion. A promising approach to meet these demands of high load flexibility, low emissions, and low flashback risk is the combustor concept of the flameless oxidation (FLOX®) where fuel and air are injected as high momentum jets, and which is described in more detail in the further sections.

Therefore, the overall scope of this paper is to investigate the potential and feasibility of the compound with emphasis on the MGT performance depending on two different solid-media storages and on a suitable combustor concept.

1.2. Literature Study

In the past years, several research groups analyzed the potential and benefits of integrating a high-temperature heat storage (HTES) in different applications. Spelling et al. amongst other groups [8–10] investigated a solar gas turbine power plant coupled with an HTES to increase the fraction of solar heat supplied to the power cycle [11]. The HTES is placed in parallel to the solar receiver allowing to store the excess solar energy during the daytime and using it in times with low solar heat thus increasing the operation time and the flexibility of the power plant. Their simulations showed that the hybrid power plant provides a 60% reduction in electricity generation costs and a 32% reduction in CO_2 emissions.

The group around Powel et al. [10] focuses on the control of a solar thermal power plant with integrated HTES and how an HTES can be leveraged to control power output despite significant fluctuations in solar radiation availability. Their studies show that by integrating an HTES the fuel demand can be reduced by 43%. Further groups have studied the combination of an HTES with a solar power plant for example the group around Kuravi et al. or Flueckiger et al. [8,9].

Moreover, several groups worked on the alignment of power or heat generation with load demand, by integrating energy storage in combined-cycle gas turbine power plants (CCGT). In the DLR project called FlegS the potential of increasing the flexibility of a combined cycle gas turbine for industrial processes was investigated by using a solid media HTES for decoupling the demand for electrical and thermal power. The idea is to run the GT during times of high demand for electricity and to use the GT waste heat for running the water-steam cycle as well as for charging the HTES. In contrast, during times of low demand for electrical energy, the required heat for the water-steam cycle is only provided by discharging the previously stored heat from the HTES without running the GT [12]. Furthermore, Li et al. pursued a numerical feasibility study of a CCGT integrated with a thermal storage system for fast dynamic responses [13]. The potential of a reduction of the plant restart-up time and the usage of the stored heat for a steam generation were studied. Besides, the integration of an HTES in a coal-fired power plant was examined by the groups around Wang et al. [14,15]. Moreover, the topic of using various storage technologies for cooling the inlet temperature of a GT compressor has been studied by several groups [16,17]. However, using an HTES to reduce the fuel consumption of an MGT with a highly flexible jet-stabilized combustor (based on the FLOX® concept) has not yet been described in the literature to the authors' best knowledge.

In principle, all HTES technologies that enable minimal losses (in terms of exergy) during heat transmission can be considered for the compound. Such technologies allow for a time-decoupled operation improvement in systemic flexibility and efficiency, and are widely investigated in stationary applications, e.g., industrial [7,18] or power plant [19,20] processes. Depending on the application, media, temperature level, or systemic requirements, sensible [21,22], latent [23,24], or thermochemically [25,26]-based thermal energy storage options are suitable. However, since the temperatures at the hot and cold ends of HTES are largely determined, only solid media storage can meet the requirements. Solutions of these solid-media storages typically consist of stacked ceramic inventory bricks (e.g., honeycomb), which are integrated directly into the flow path as illustrated in Figure 1, whereas no additional heat exchanger structures are required. Such regenerator-type options enable together with efficient thermal insulations high systemic storage densities—due to the use

of ceramic materials suitable for high temperatures—and reach high discharging powers—due to high specific heat transfer surfaces, as well as direct contact between the solid and the fluid phase. Technological developments in terms of an appropriate high-temperature electric heating system are shown in [27], offering a powerful resistance-based and efficient charging through thermal radiation at high operating temperatures of up to 1300 °C and homogeneous heating of the inventory. Alternative electric heating technologies such as inductive processes [28] enable further operational flexibilities if adequate materials are selected but are linked with significantly higher demand for electrothermal designing.

As mentioned in the introduction, a promising approach to meet the demands of high load flexibility, low emissions, and low flashback risk are combustion systems based on the idea of flameless oxidation (FLOX®), also known as volume or MILD combustion [29,30]. This concept was adapted for use in MGT systems. Within the MGT systems, the combustion is as well stabilized via recirculation caused by high-momentum jets, but the combustor itself usually does not operate in the flameless regime. Within the past years, the DLR Institute of Combustion developed and tested several jet-stabilized combustors for various MGT applications. They differ with respect to thermal input (20 to 1000 kW), numbers of fuel nozzles (six to twenty), used fuel (natural gas, wood gas, biogas, hydrogen, . . .), combustor inlet temperature (873 to 1123 K) or combustor stages. Systems suitable for MGTs with typical MGT combustor inlet temperatures (in the range of 873 K) are, e.g., presented in [31–36]. Furthermore, jet-stabilized combustors for elevated inlet temperatures have been developed and proved their suitability for the MGT-HTES power plant application by their stability and low emissions potential, e.g., in an MTT EnerTwin CHP system with combustor inlet temperatures up to 1000 K (NO_X < 10 ppm, CO: about 5 ppm at base load and about 100 ppm at part load). Although, the combustor inlet temperature was above the self-ignition temperature of natural gas and fuel and air were technically premixed, no flashback events were observed. Besides, the combustor proved its fuel flexibility with biogas [37]. For even higher combustor inlet temperatures of up to 1123 K, a combustor for SOFC off-gas with a very low lower heating value of 1–3 MJ/kg has been developed [38]. More detailed information about the various jet-stabilized combustors can be found in [39–42]. However, there is no combustor for natural gas for a combustor inlet temperature range of 973 K to 1153 K available.

1.3. Scope of Work

The idea of this paper is to integrate an HTES in an MGT-based CHP unit to store off-demand produced power as heat and reconvert and supply it on-demand, and introduce a jet-stabilized combustor (based on the FLOX® principle) to ensure a stable and environmentally friendly operation of the compound.

The overall goal of this paper is to pursue a fundamental potential and feasibility analysis of the compound regarding performance and combustor emissions and operating range. Hence, a numerical cycle analysis investigating the influence of the HTES on the MGT is pursued. Based on these results, the first requirements for a combustor design are derived. Moreover, the development of a highly load-flexible and low-emission combustor for the compound is addressed. Designing a highly efficient and economic feasible MGT-HTES power plant can be a complex task since there are many technical design parameters (e.g., storage capacity, discharging process, operating concept) to consider that strongly depend on the applications field (energy consumption and load profile), as well as on the political and economic boundary conditions (e.g., availability of renewable electricity, pricing). Since these studies represent the first development step, they are performed application independent.

The presented paper is divided into three sections. First, the influence of the HTES on the MGT components with a focus on the combustor and compound operation is qualitatively analyzed. Subsequently, in the methodology section, in-house cycle simulation tools, derived models, and their modifications for this study, as well as applied boundary conditions for the calculations, are described. Additionally, an overview of the exper-

imental test rig and its instrumentation is given. Finally, the results are discussed. In the thermodynamic cycle analysis, the influence of two different HTES parameter sets, representing a solid-based HTES with low and high specific heat transferring areas, on the MGT performance (e.g., fuel consumption, efficiency) are examined. Moreover, preliminary considerations of the influence of the HTES on the combustor as well as the stable operating range and the CO and NO_X emissions for different primary air ratios (PAR) are presented.

2. Qualitative Analysis and Challenges of the Compound

In the presented compound, the HTES is placed between the recuperator outlet (air-side) and the combustor, increasing the combustor inlet temperature and thus reducing the necessary fuel mass flow when considering a constant combustor outlet temperature. Here, the HTES is based on a solid media thermal energy storage system consisting of ceramic inventory bricks (e.g., honeycomb). During the charging period, the required heat is generated through an electrical high-temperature heating system, stored inside the solid medium, and transferred during discharging operation in direct contact with the MGT process medium (air). Subsequently, the combustor increases the fluid temperature from the HTES outlet temperature ($T_{HTES,fluid,out}$) to a given turbine inlet temperature (TIT). For each load point of the MGT, the maximum value of TIT is limited to prevent turbine damage. Consequently, TIT also represents the upper limit of the acceptable HTES outlet temperature ($T_{HTES,fluid,out}$). When TIT equals $T_{HTES,fluid,out}$, which is energetically the ideal case for the compound, no combustion takes place. They can be considered fully load when the average temperature of the HTES and $T_{HTES,fluid,out}$ is equal to TIT. In this study the HTES is defined as "empty" when no fluid temperature increase occurs through the HTES, so when $T_{HTES,fluid,out}$ equals to $T_{rec,air,out}$. For clarification, an exemplary fluid temperature profile at the storage outlet as a function of time and the two boundaries' temperatures (TIT and $T_{rec,air,out}$) are shown in Figure 2. The temperature profile presents one discharge cycle of the HTES. At the beginning of the discharge process, $T_{HTES,fluid,out}$ corresponds to the TIT. In the course of the discharge process, first, the upstream HTES inventory cools down, which has no effect on $T_{HTES,fluid,out}$. Then, as the most downstream storage inventory starts to emit heat, $T_{HTES,fluid,out}$ decreases down until it finally meets $T_{rec,air,out}$. The characteristics of the temperature profile depend on the design of the storage and on the process it is embedded in. When all MGT parameters remain the same and the TIT decreases, the power output of the MGT drops. To achieve a constant power output while discharging the storage, the difference between $T_{HTES,fluid,out,}$ and the TIT has to be overcome by gradually increasing the fuel mass flow up to the standard mass flow of the MGT (without HTES), which is indicated by the right vertical arrows in Figure 2.

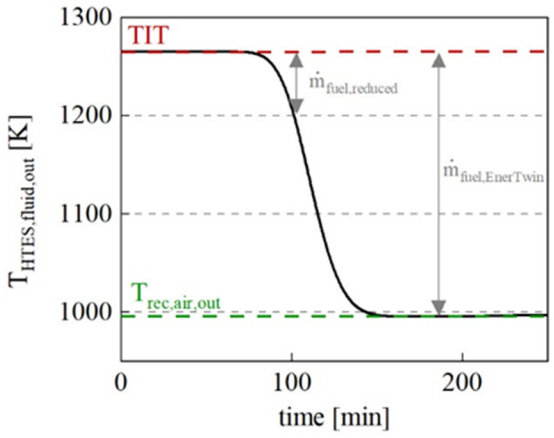

Figure 2. Exemplary HTES outlet temperature profile as a function of time within the temperature boundaries of the EnerTwin MGT.

2.1. Combustor

Combustor designs are normally optimized for a specific scope regarding inlet temperature, flow speed, thermal output, etc., in order to meet requirements like emissions and operation reliability. The changed boundary conditions present some challenges for the combustor. In the MGT HTES compound, the operation range is wider than for the stand-alone MGT. The combustor needs to be able to ignite and operate at ambient temperature when starting the MGT, up to temperatures close to the TIT level. Depending on $T_{HTES,fluid,out}$, only a small rise in temperature and a hence small amount of fuel mass flow in the combustor is necessary, to reach the required TIT. Since, the air mass flow of the MGT is independent of $T_{HTES,fluid,out}$ and stays the same, a decrease in fuel mass flow leads to leaner combustion, which can result in combustion instabilities. Moreover, when operating the combustor close to the lean blow out achieving acceptable carbon monoxide emissions becomes challenging. Moreover, the increased combustor inlet temperature results in an increase in flow velocity at the combustor nozzles, which must be considered during the design process. On the one hand, since the combustor operates above the self-ignition temperature of natural gas, premixing fuel, and the air is challenging and locally low axial velocities must be avoided to decrease the risk of a flashback. On the other hand, non-premixed combustion leads to high local combustion temperatures which promote thermal NO_X formation. Consequently, thorough studies and significant changes to the combustor design might be necessary to meet the changed requirements, realize safe and reliable combustion and low pollutant emissions.

An important design parameter to control the combustion characteristics of MGT combustors is the primary air ratio (PAR) within the combustion system. In MGTs, only a part of the air mass flow participates in the actual combustion as so-called primary air. The larger part of the air, the so-called secondary air is used as dilution air at the end of the combustion chamber to cool down the flue gas before entering the turbine. The ratio between those air flows which is defined as

$$PAR = \frac{\dot{m}_{air,\ primary}}{\dot{m}_{air,\ primary} + \dot{m}_{air,\ secondary}} \quad (1)$$

Figure 3 depicts a schematic MGT combustion chamber system with a jet-stabilized combustor. In the present combustor, the air/fuel mixture is injected into the combustion chamber via twelve circumferential arranged nozzles. Within the air/fuel-nozzles, the fuel is injected co-axially into the primary air and technically premixed within the mixing section before entering the combustion chamber. The air/fuel mixture enters the combustion chambers with high momentum which generates (in combination with the surrounding geometry) a strong inner recirculation zone. This inner recirculation zone dilutes the incoming fresh air with flue gas which leads to a homogeneous temperature without local temperature peaks, which is essential for low NO_X emissions. Due to the high axial velocity of the air/fuel mixture, the risk for flashback is significantly reduced, even for very high inlet air temperatures. Therefore, the jet-stabilized concept is particularly suitable for application in the combined heat storage micro gas turbine cycle.

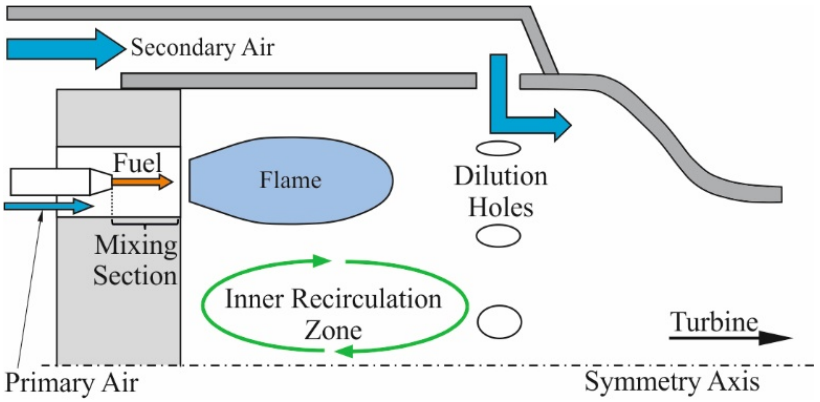

Figure 3. Schematic of jet-stabilized combustion principle in MGT configurations.

2.2. Turbomachinery and Heat Exchangers

For the turbomachinery no major influences of the HTES can be expected in steady-state operation since the temperature at the compressor and the set temperature of the turbine inlet for a single operating point are the same as for the conventional MGT. Moreover, as natural gas is used, depending on the type of MGT the fuel mass flow is very low in relation to the total mass flow. For example, at full load, the fuel mass flow of the EnerTwin by MTT accounts for 1% of the total mass flow. Hence, no significant changes in the operating point of the turbine are expected for the compound. However, for low-caloric fuels, the impact can be significant. As the HTES introduces additional gas volume to the system slightly adapted startup and shutdown maneuvers might be necessary to prevent compressor surges.

The additional pressure loss of the storage is very small compared to other components in the MGT (e.g., recuperator), see Tables 1 and 2. Hence, only a small impact can be expected. Moreover, since TIT remains the same, the recuperator temperatures at the inlet and outlet of the air and exhaust gas side are not influenced by the HTES. The same applies to the water heat exchanger. Hence no major influence of the HTES on these components is expected.

2.3. Operation of the Compound

When the HTES is fully charged ($T_{HTES,fluid,out}$ = TIT) and the CHP unit is turned on, the MGT simply operates without combustion. When $T_{HTES,fluid,out}$ < TIT, fuel is added to maintain constant power output. When $T_{HTES,fluid,out}$ is just slightly below TIT and thus the fuel flow would be too low for the combustor, the shaft speed could also be temporarily lowered, as the optimal TIT is lower in part load operation and the reduction of electrical efficiency is smaller in comparison to a TIT reduction at maximum shaft speed. When the storage is empty the compound operates like a stand-alone MGT since the pressure and heat losses of the HTES can be neglected.

When the $T_{HTES,fluid,out}$ corresponds to the TIT of the MGT at full load, the MGT cannot be operated at part load since the maximum recuperator inlet temperature at the exhaust side would be exceeded. So, depending on the $T_{HTES,fluid,out}$ the operating point (shaft speed) needs to be selected accordingly. Hence, a bypass valve, e.g., from the compressor outlet to the combustor inlet might be necessary to broaden the operation range and reduce stress on the recuperator during the start-up.

When the storage is cold (ambient temperature), it needs to be considered if it is technically and economically feasible to charge the storage to more than 1000 K with the MGT or with electricity from the grid. In case there is no design solution for a combustor covering the whole temperature range, for starting the MGT at ambient conditions when the HTES is cold the combustor air could be preheated with an additional heating element or the HTES heating device could be designed to enable separated heating of the most downstream segments while wasting no electrical energy on the segments further upstream.

These topics need to be addressed when designing a compound for a specific application. The operating range of the combustor is discussed further down.

Based on the results of the qualitative analysis, it can be said that there are two main aspects that should be addressed in the first potential analysis of the compound: firstly, the investigation of the benefit of the HTES on the MGT considering different storage designs thus temperature profiles and secondly the development of an adapted combustor and investigation of the operating range and emissions.

3. Methodology

3.1. Cycle Analysis

For the investigation of the system during the HTES discharge process, transient numerical simulations are necessary. It can be assumed that the relevant time constants of the system components are within a wide range. Compared with the time constant of the heat storage, those of the MGT (shaft, fluid dynamics, recuperator) are very small. Therefore, a fully transient simulation must ensure small time steps compared to the investigated time range of the simulation to cover all relevant transient processes. This results in a large computation effort. However, the system can be simplified using the assumption, that the time constant of the heat storage is much larger than that of the MGT. Thus, only the heat storage has to be simulated transiently, while quasi-stationarity can be assumed for all other components. Except for transient maneuvers (e.g., switch-on/off processes), the errors caused by this simplification are expected to be negligible. Hence, these adaptions were conducted for this paper. The simulations are performed with the DLR in-house simulation environment MGTS^3 (Micro Gas Turbine Steady State Simulator). It is a Matlab/Simulink-based, robust and fast simulation tool, developed by the Institute of Combustion Technology of the DLR, able to compute steady-state systems with arbitrary interconnections between components. The MGTS^3 tool is based on the work of Panne et al. [43] and was extended with detailed component models (e.g., recuperator, WHX) by Henke et al. [44]. Furthermore, Krummrein et al. developed a new solver routine enabling a highly flexible and robust computation of complex systems [45]. The tool has been used for the investigation of various thermodynamic MGT cycles (e.g., Inverted Brayton Cycle [46], MGT-SOFC hybrid power plant [47]). The process gas is considered to be an ideal gas. The isobaric heat capacity is considered as a function of temperature, based on a five-coefficient polynomial [48]. The components as well as the piping between the components are represented by physical 0D models allowing heat and pressure loss consideration for each component in various levels of detail [47,49]. The turbomachinery quantities are typically represented by maps or can be either specified by the user or determined by the MGTS^3 solver. The heat exchangers are specified by a constant efficiency. Mechanical losses of the shaft are assumed to be linear to the shaft speed whereas conversion losses of the generator and power electronics are summarized as a linear function of the shaft power.

3.1.1. MGT

The power output range of commercially available MGT CHP units varies from 3 kW_{el} like the EnerTwin developed by the Dutch company Micro Turbine Technology up to 400 kW_{el} like A400 developed by Finnish company Aurelia. The here presented numerical investigations are based on the EnerTwin since these studies serve as a basis for an experimental investigation that is planned to be pursued on the DLR EnerTwin test rig. At full load conditions, the EnerTwin has a nominal shaft speed of 240 krpm, an operating range of 180–240 krpm, an electrical efficiency of 15%, overall efficiency of 90% and the maximum pressure ratio of the compressor is about 3:1 [50]. The power module is characterized by a single stage, single shaft turbomachinery with radial impellers with the generator located in between the compressor and turbine as illustrated in Figure 1. Further information about the EnerTwin can be found in [50–52].

In previous projects, all relevant parameters of the EnerTwin like the efficiencies, heat and pressure losses of the main components and piping, as well as mechanical and

conversion losses were experimentally determined. Based on the experimental data the simulation tool was parameterized and validated. Furthermore, turbomachinery maps were generated from experimental data which are also implemented in the simulation tool. These parameters are also used for the cycle analysis in this paper and an excerpt of them is given in Table 1. Compressor inlet conditions were set for all simulations to dry air conditions with an air temperature of 288 K and an ambient pressure of 1.013×10^5 Pa. The pressure loss is given relative to the inlet pressure of the component.

Table 1. Excerpt of MGT model input parameters derived from experimental data of the DLR test rig at 240 krpm (full load point).

Component	Value
$\Delta p_{Recu,air\text{-}side}$	3.1%
$\Delta p_{Combustor}$	3%
$\Delta p_{Recu,exhaust\text{-}side}$	2.7%
Δp_{WHX}	0.2%
η_{Rek}	89%
η_{WHX}	95%
TIT	1265 K

3.1.2. HTES

While discharging the HTES, the temperature outlet characteristic is based on the effectiveness of thermal transport between the previously electrical heated solid medium and the inventory passing fluid. Central influences for this are relating especially to geometrical aspects of the inventory (specific heat transport area, void fraction), whereas the storage mass is linked to the discharging duration. Additionally, material properties and area-specific mass flow rates play a significant role in the resulting temperature characteristics and must be regarded inside the modeling approach.

For calculating the temporal t and spatial z temperature profiles of the fluid T_{fluid} and the solid T_S, a heterogeneous porous thermal model can be used [53], which is provided by the Institute of Technical Thermodynamics of the DLR. Based on the idea to create an "easy-to-implement" HTES tool for gas turbine system simulations, simplifications are performed to formulate a compact HTES model [7]. Such simplifications include negligence of radial gradients, of thermal diffusion effects—well justified for the ceramic materials under investigation due to their low heat conductivities—and the assumption of constant material properties. After normalization in space, z* the resulting one-dimensional heat balances for the fluid and solid phase in the axial direction can be written as

$$\frac{\partial T_S}{\partial t} = \Pi_D (T_{fluid} - T_S) + \Psi (T_U - T_S) \quad (2)$$

$$\frac{\partial T_{fluid}}{\partial z^*} = \Lambda (T_S - T_{fluid}) \quad (3)$$

This formulation describes the thermal behavior of the solid with only three parameters: the reduced period duration Π_D, the reduced length Λ and the reduced heat loss Ψ to the environment (T_U). These parameters include as central values the heat transfer surface between the storage inventory and the heat transfer fluid, the total storage mass, the mass flow rate, and the specific heat capacities, as well as the total heat transfer coefficient between the solid and the fluid regarding the thermal conduction resistance inside the inventory, defined as given by [54]. Both differential equations are solved numerically by using a backward finite-difference-method in space and time. The resulting expressions are implemented in a HTES function with input parameters-mass flow rate and fluid inlet temperature—defined by the MGT process and with an output parameter-fluid outlet temperature ($T_{HTES,fluid,out}$)—defined by the HTES parameters.

For the performance analysis of the system under investigation, two commercial inventory options are defined, both based on low-cost ceramic refractory materials with low heat conductions:

- Checker brick with low specific heat transport surface (a_v = 56 m^2/m^3) and low void fraction (ε = 30%)
- Honeycomb with very high specific heat transport surface (a_v = 1350 m^2/m^3) and high void fraction (ε = 68%)

For both inventory options, a storage capacity of 40 kWh was defined assuming maximum (homogenous) temperatures at the end of electrical charging of 1273.15 K and minimum temperatures at the end of discharging of 975 K. With additional assumptions regarding the length to diameter ratio of the HTES (L/D = 2) and the negligence of heat losses (Ψ = 0), the HTES parameters Π_D and Λ were determined and parametrized in terms of the mass flow rate.

Although the electric heating system and charging procedure are not focused on in this paper, different types of commercial high-temperature power-to-heat technologies are feasible, mostly based on ceramic or metal resistance heating elements (Joule heating) [27]. Additional to those commercial products, alternative material options, designs, and technologies (e.g., inductive heating [28]) are investigated in different R&D projects at the Institute of Technical Thermodynamics.

The two different HTES parameter sets that are examined in this paper are listed in Table 2. The resulting temperature profiles ($T_{HTES,fluid,out}$) are given in Figure 5 and discussed further down in this paper.

Table 2. Parameters of the HTES models for the different case studies.

	m	**Q**	**H/D**	**V**	$\mathbf{a_v}$	ε	Δp_{HTES}
Case 1: checker bricks	363 kg	40 kWh	2	219 l	30%	56 m^2/m^3	4.2 Pa
Case 2: honeycomb bricks				480 l	68%	1350 m^2/m^3	140 Pa

3.2. Combustor Development

The combustor design is a further development of a six-nozzle jet-stabilized combustor suitable for a micro gas turbine with an electrical power output of 3 kW and a combustor inlet temperature of approximately 1000 K, which is presented, for example in [37,39].

The development of the presented combustor was supported by computational fluid dynamics (CFD) simulations that were performed for the atmospheric test rig setup. Since this is not in the scope of the present paper, the results are not shown here.

For the experimental investigation of the combustor, an atmospheric test rig with optical access was used. These test rigs offer the advantage to investigate the combustion characteristics of the combustor without limitations due to the MGT operation conditions. The air and fuel mass flows, as well as the combustor inlet temperature, can be varied independently of each other. Since the dilution air is ideally added downstream of the reaction zone in order to avoid affecting the combustion (e.g., quenching), the secondary air mass flow is neglected for these tests. In this test rig, the air is electrically preheated to the desired inlet temperature, which is determined by the average of three thermocouples (type N, tolerance class 1) shortly upstream of the combustor. Their axial position can be seen in Figure 4. Within this paper, the combustion inlet temperature $T_{cc,in}$ is assumed to equal the heat storage outlet temperature ($T_{cc,in} = T_{HTES,fluid,out}$).

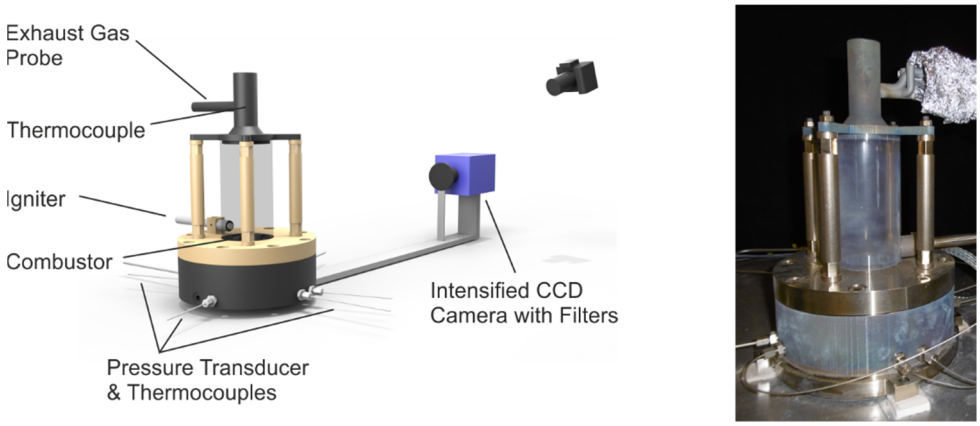

Figure 4. Setup of the atmospheric test rig [55] and combustor with the used optical combustion chamber.

The flue gas was extracted by a probe in the exhaust gas duct of the combustion chamber as shown in Figure 4. For the determination of the lean blow-off (LBO) a thermocouple in the exhaust stream near the exhaust gas probe position was used. The spark plug igniter in the lower part of the combustion chamber is only used for igniting the incoming air/fuel mixture prior to the measurements.

The flame shape and location were determined based on OH* chemiluminescence by applying an intensified CCD camera with filters, though the results are not part of this paper.

Since the MGT is operated at pressures up to approximately 3 bar, the difference in pressure level between the atmospheric test rig and the MGT was considered by scaling all mass flows according to

$$\dot{m}_{ATM} = \dot{m}_{MGT} \cdot \frac{p_{ATM}}{p_{MGT}} \tag{4}$$

In order to keep Mach number similarity (and therefore similar flow velocities, residence times, and pressure losses), constant heat capacity ratios and similar fluids, geometry, and combustor inlet temperatures are assumed in Equation (4).

The combustion is characterized by the air number λ which is defined as the reciprocal value of the equivalence ratio ϕ and is calculated with the air mass flow $\dot{m}_{air}$, the fuel mass flow $\dot{m}_{fuel}$ and the stochiometric air fuel ratio AFR_{st} according to

$$\lambda = \frac{1}{\phi} = \frac{\dot{m}_{air}}{\dot{m}_{fuel} \cdot AFR_{st}} \tag{5}$$

Alternatively, the air number can be calculated by the measured (volumetric) residual oxygen content X_{O_2} of the flue gas via

$$\lambda = \frac{1}{\phi} = \frac{20.95}{(20.95 - X_{O_2})} \tag{6}$$

In order to explore the stability limit, lean blow-off was investigated by increasing the air mass flow automatically at constant thermal power with a ratio of $\Delta\lambda$ = 0.04 1/s. The lean blow-off was defined as the point with maximum temperature gradient and to quantify the lean blow-off conditions, the data were averaged for 15 s prior to maximum temperature gradient. This procedure was repeated three times and the results were averaged.

Furthermore, the adiabatic flame temperature T_{ad} was calculated for LBO, as well as for different stationary load points. The adiabatic flame temperatures were calculated using the simulation software Chemical WorkBench (version 4.1.19528 from Kintech Lab Ltd., Moscow, Russia) assuming constant enthalpy and isobaric conditions with the GRI3.0 as the reaction mechanism with the equivalence ratio ϕ calculated according to Equation (6).

4. Results

4.1. Numerical Results

The overall goal of the numerical studies is to examine the influence and benefit of different HTES types on the MGT performance and derive the first requirements for a combustor design. For these studies, process simulations of the compound for one discharge cycle of the HTES are conducted, based on the model parameters of the two exemplary different HTES configurations given in Table 2, and the performance data are compared. As a reference case for comparing the influence of the HTES on the MGT serves the calculated performance data of the stand-alone MGT is given in Table 3. It should be noted that these values represent the performance data of our test rig which is based on an early-stage prototype of the EnerTwin.

Table 3. Simulated performance data of the MGT at full load.

Parameter	Value
Π_{Comp}	3.1
$\eta_{Turb,isen}$	73.4%
P_{el}	2.6 kW
P_{th}	11.6 kW
P_{fuel}	17.8 kW
η_{el}	14.8%
η_{ov}	80%

As mentioned above, the heat losses of the HTES are neglected and the starting solid temperature is set to 1265 K (full load point) for all HTES cases, corresponding to the TIT of the MGT when operated at full load. For the following discussion only $T_{HTES,fluid,out}$ is considered since the solid temperature is not directly relevant to the performance data of the MGT. The MGT component parameters are not varied and are listed in Table 1. For the air at the compressor inlet, dry air is used. The water inlet temperature of the WHX is set to 303 K and the water mass flow rate is controlled to reach a water outlet temperature of 323 K. Since the minimum fuel mass flow of an optimized combustor in terms of operating range is not known yet, for simplification it is assumed that the combustor can be operated with any small amount of fuel mass flow. The following discussions are pursued for the full load point of the MGT since the qualitative course of $T_{HTES,fluid,out}$ is the same for any load point.

Figure 5 (left side) shows the resulting temperature profiles ($T_{HTES,fluid,out}$) for HTES configurations as a function of time. At the beginning of the discharge process, the $T_{HTES,fluid,out}$ of the checker bricks HTES (red curve, case 1) does not reach the temperature of the solid, which is 1265 K, and reaches only 1254 K. The reason is that checker bricks have a coarser structure with a smaller specific heat transfer surface and a lower porosity than honeycomb bricks. Hence the heat transfer with the state-of-the-art checker bricks is not sufficient to exploit the temperature potential. In contrast to the HTES with honeycomb bricks (blue curve, case 2) $T_{HTES,fluid,out}$ reaches the maximum temperature of the solid due to the heat exchange properties of the bricks. Moreover, the temperature drop occurs in a shorter time period, hence the discharge duration for the same stored heat amount is shorter. It should be noted that the discharge duration time is also a function of the heat capacity and other design parameters of the HTES that are not varied or considered in this study. The discharge time, defined here as $T_{HTES,fluid,out}$-$T_{rec,air,out}$ < 1 K, accounts for 600 min for case 1 and 258 min for case 2.

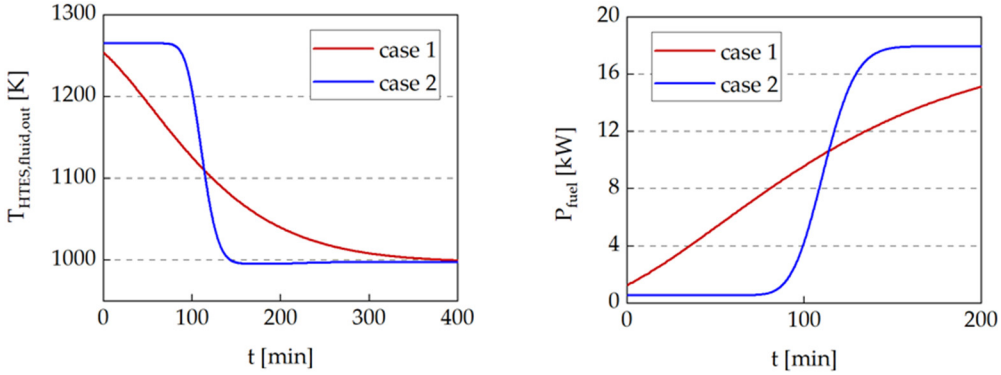

Figure 5. (**Left**): Temperature profiles of different HTES set ups presented in Table 2, (**right**): influence of the different HTES cases on the fuel demand of the MGT as a function of time.

As a next step, the influence of the different temperature profiles on the fuel demand (shown in Figure 5, right side), as well as on the thermal and electrical power output of the MGT are examined. For both cases, the fuel demand at the beginning of the discharge process is low and increases over time up to 17.8 kW which corresponds to the demand of the stand-alone MGT. In the simulations fuel demand is never zero, even at starting time of case 2. This is to compensate the 550 W of heat loss occurring in the combustion chamber. In a real application this could be avoided by allowing a $T_{HTES,fluid,out}$ slightly above the TIT. For the HTES with checker bricks the temperature difference between $T_{HTES,fluid,out}$ and TIT is compensated. Hence, P_{fuel} accounts for 1.3 kW for case 1 (red line) at the beginning of the discharge cycle.

At the beginning of the discharge cycle, the thermal power output (P_{th}) is about 8% lower than P_{th} of the stand-alone MGT. Due to the change in gas composition and smaller mismatch between the mass flow of the air and exhaust gas side within the recuperator, the outlet temperature of the exhaust gas side of the recuperator is about 10 K lower in comparison to a conventional MGT operation. Consequently, thermal power output during discharge in the subsequent water heat exchanger is reduced.

To better compare the influence of the different temperature profiles of the HTES on the MGT performance, the main performance parameters for the specific discharge duration of the cases (for one discharge cycle) are averaged (see Table 4). As it can be seen the average electrical power output ($P_{el,ave}$) of the compound is hardly affected by the HTES. The average thermal power output ($P_{th,ave}$) is 100 W lower for case 1 and 400 W lower for case 2 compared to P_{th} of the stand-alone MGT. When calculating efficiencies, the same way as for a stand-alone MGT arithmetically values above 100% may occur. For the average performance, both HTES cases are beneficial for the compound. Fuel savings can account for up to 42% (case 2) of the given discharge duration leading to lower emissions and operating costs for the power plant.

Table 4. Averaged performance parameters of the compound for one HTES discharge cycle.

	Case 1	**Case 2**
$\Delta t_{discharge}$ [min]	600	258
$P_{el,ave}$ [kW]	2.62	2.59
$P_{th,ave}$ [kW]	11.5	11.2
$P_{fuel,ave}$ [kW]	14.5	10.4
$\eta_{el,ave}$ [%]	18	24.8
$\eta_{ov,ave}$ [%]	97.3	132.6
$\Delta m_{fuel,saved}$ [%]	18	42

The MGT-HTES power plant reaches a higher electrical and overall efficiency when $T_{HTES,fluid,out}$ exhibits a short and sharp temperature decline, which is the case for the HTES with honeycomb bricks due to their high porosity and a high specific surface. This is true

when only looking isolated at one discharge cycle. However, when comparing both HTES cases in regard to the average fuel consumption of the compound for a fixed timeframe (so when HTES is first discharged and then the MGT is operated in stand-alone mode for the rest of the time), the above-described benefit vanishes. Regarding fuel consumption, this is the case after 9.64 h (the breakeven point) for the presented cases. Consequently, which HTES type is more beneficial strongly depends on how the discharge duration and frequency are matched with operation durations and energy demand of an application.

General Combustor Requirements

Based on the numerical studies, the process parameters and requirements for an ideal combustor design and experimental investigation can be derived:

- Fuel mass flow range: nominal fuel mass flow (0.38×10^{-3} kg/s) when the storage is empty and as low as possible while the HTES is being discharged
- Combustor inlet temperature: 973 K to 1265 K during operation and 293 K during start-up or when the HTES is cold
- Combustor inlet pressure: 1×10^5–3×10^5 Pa

However, realizing a combustor that can operate stably for such a wide temperature range while having low pollutant emissions is quite challenging, as described further down in the paper. These requirements can be stretched when ensuring combustor inlet temperatures above 973 K (for example by an additional heating element).

4.2. Combustor Results

4.2.1. Parameter Range

The boundary conditions for the combustor tests are shown in Table 5. The combustion chamber inlet temperature $T_{cc,in}$ was varied between 973 K and 1153 K. In general, four different primary air ratios, from 18 to 26.4%, were investigated. Due to test rig limitations, the maximum preheat temperature of 1153 K could only be reached for PAR = 23% and 26.4%. The measurement points correspond to load points within the stationary operation range of the MGT (N = 180–240 krpm). Therefore, all mass flows (and thus thermal powers) were scaled to atmospheric conditions according to Equation (4).

Table 5. Test conditions for atmospheric test rig.

Parameter	Values
$T_{cc,in}$ [K]	973/1073/1113/1153
PAR [%]	18/20/23/26.4
N [krpm]	180 . . . 240
λ [-]	1.6 . . . LBO

4.2.2. Stable Range of Operation-Numerical Investigations

As seen above, the combustion system of the MGT needs to cover an enlarged stationary operating range when used in combination with an HTES. In order to obtain an impression of the expected combustion conditions, the adiabatic flame temperature T_{ad} and the air number λ were calculated for different primary air ratios PAR and HTES fluid outlet temperatures $T_{HTES,fluid,out}$ (which correspond in this paper to the combustor inlet temperature $T_{cc,in}$).

Figure 6 shows these parameters for combustion chamber inlet temperatures of 673 K, 973 K, 1073 K, 1173 K for a primary air ratio of PAR = 20%, exemplarily.

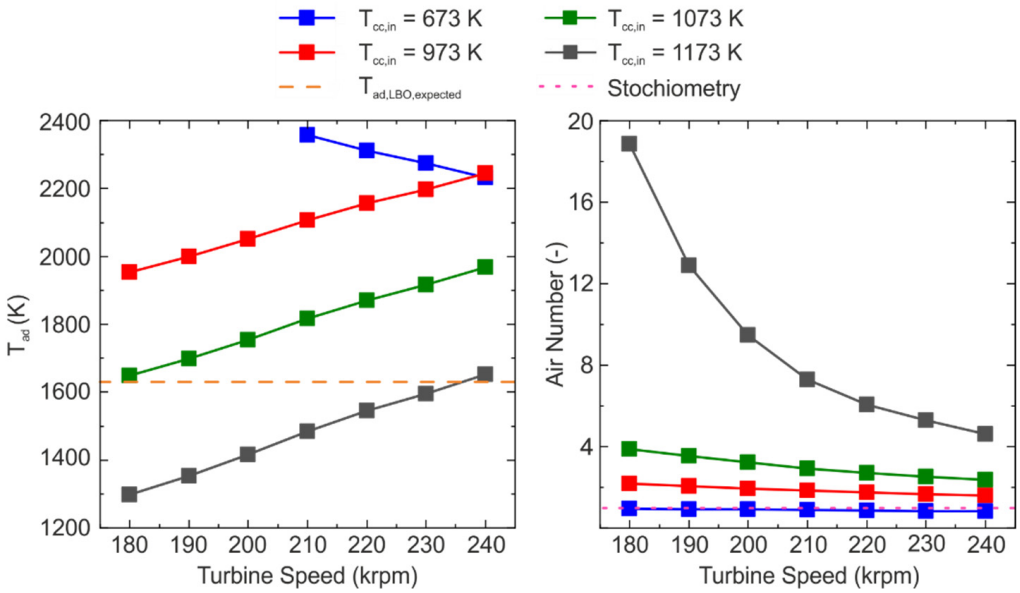

Figure 6. Adiabatic flame temperature and air number for a primary air ratio of PAR = 20% for different combustion chamber inlet temperatures.

With increasing turbine speed, the combustion becomes less lean indicated by a decreasing air number. For all steady load points, the maximum temperature at the recuperator inlet is the most limiting factor regarding cycle temperatures. Hence, the fuel mass flow of the MGT is controlled to always reach this maximum temperature. Consequently, increasing turbine speed and pressure ratio will enable higher turbine inlet temperatures and thus lower air number values for a given $T_{cc,in}$. At a combustion chamber, the inlet temperature of 1173 K and a PAR of 20% the air number increases from base to part load, from approximately 4.6 to almost 19, accompanied by a decrease in adiabatic flame temperature from 1653 to 1297 K. Previous studies of a similar combustor (but with six nozzles) indicated lean blow-off at an adiabatic flame temperature of approximately 1630 K at comparable combustion chamber inlet temperatures of 1000 K [39]. Therefore, the occurrence of lean blow-off is expected at similar combustion temperature levels. This temperature limit is shown in Figure 6 as a solid orange line. For a primary air ratio of PAR = 20%, stable combustion within the complete stationary operation range is expected for heat storage outlet temperatures of 973 K and 1073 K. At 1173 K base load seems possible, at least in terms of stability. Due to the low adiabatic flame temperatures, it can be assumed, that part load is not feasible. Therefore, as the first development step, in this study, only temperatures up to 1173 K are considered.

As Figure 6 shows, combustion at $T_{cc,in}$ = 673 K is not feasible for PAR = 20% as too little air enters the combustor to oxidize the fuel and hence the desired outlet temperature cannot be reached. Hence, the compound could not be operated with this $T_{cc,in}$ at this PAR. Here, for example, an additional electrical heating element could be integrated into the HTES design to elevate $T_{cc,in}$ when a cold start is performed.

Thus, the combustor inlet temperature accounts at least for 973 K corresponding to the standard $T_{cc,in}$ of the stand-alone MGT or the case where the HTES is considered "empty". This is the lowest $T_{cc,in}$ that is taken into account for further experimental investigations within the present study.

Apart from the shown case of PAR = 20% in Figure 6, primary air ratios of 18%, 23%, and 26.4% have been investigated numerically. The general trends are listed in Table 6.

Table 6. General trends for PAR change on stability, air number λ, and thermal load on material.

	Air Number λ	High $T_{HTES,Fluid,out}$ and/or Part Load	Low $T_{HTES,fluid,out}$ and/or Base Load	Thermal Load on Inner Walls
PAR increase	increase	risk of LBO	reduced risk of $\lambda < 1$	decrease
PAR reduction	decrease	more stable	risk of $\lambda < 1$	increase

An increase in PAR results is an increase in air number and therefore in an increased risk of LBO at high $T_{HTES,fluid,out}$, while the thermal load on the inner combustor walls decreases. A decrease in PAR means more stable combustion at high $T_{HTES,fluid,out}$ and/or part load, but involves a higher risk of fuel-rich combustion conditions at low $T_{HTES,fluid,out}$ and/or base load, accompanied by an increased thermal load on the combustor parts. Hence, choosing a PAR is a trade-off between material load, fuel-rich combustion, and enabling combustion with even higher $T_{HTES,fluid,out}$. Additionally, as shown in the following paragraph, achieving low pollutant emissions has to be considered within this PAR trade-off process.

4.2.3. Stable Range of Operation-Experimental Investigations

In order to verify the above-discussed numerical investigations and assumptions and to determine the carbon monoxide (CO) and nitrogen oxide (NO_X) emissions, all primary air ratios are considered in the experimental investigation. The procedure of determining the limit of the stable operation range (lean blow-off limit) is described in the methodology part. The adiabatic temperature at LBOs for different combustor inlet temperatures $T_{cc,in}$ are shown in Figure 7 by circles in the corresponding color.

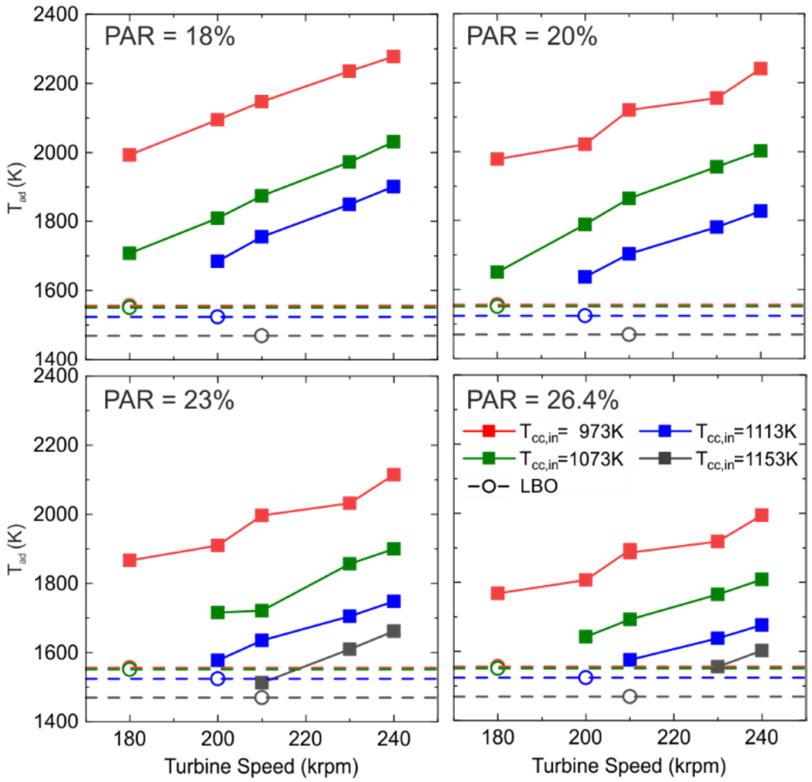

Figure 7. Adiabatic flame temperature T_{ad} of investigated stationary load points and at lean blow-off limits.

While the filled points show the adiabatic flame temperature of the investigated stationary load points at different PAR, the unfilled circles show the adiabatic flame temperature at lean blow-off.

Since the leanest conditions at each combustor inlet temperature occur at part load, the LBO was investigated at the lowest turbine speed with stable combustion within the tested PAR range. It should be noted that $T_{ad,LBO}$ is the same for all four subfigures since the thermal power was held constant while the air mass flow was continuously increased until LBO occurred. Therefore, this procedure corresponds to a variation in PAR and is hence independent of a specific PAR.

As expected, with increasing PAR, the adiabatic flame temperature decreases for constant $T_{cc,in}$, and limits the possible operation range to higher turbine speeds. The same trend is observed for increased $T_{cc,in}$ at constant primary air split. Though former investigations indicated, only a small influence of thermal power on the LBO air number λ_{LBO} [39], the thermal power seems to have a slight influence on the minimum adiabatic flame temperature for maintaining combustion. At $T_{cc,in}$ = 973 K, the adiabatic flame temperature at LBO is indeed lower than expected from previous developments, and therefore, slightly lower turbine speeds at high combustor inlet temperatures are possible with this combustor. In addition, with increasing inlet temperature, the minimum stable adiabatic flame temperature decreases which also supports a wider operating range in terms of combustion stability. However, in general, with rising combustor inlet temperatures, the stable operating range is limited to higher turbine speeds. As mentioned above 1113 K and 1153 K could only be realized for PAR = 23% and 26.4%.

4.2.4. Emissions

Besides combustion stability, NO_X and CO emissions are crucial for combustor development, since they are limited by regulations. These exhaust gas species are shown in Figures 8 and 9, respectively. The uncertainty is shown by error bars at each measurement point. Depending on the scaling of the y-axis and often rather low absolute errors, the upper and lower error bars overlap in some measurement points and appear almost as a single line. Since the upper limit of the CO analyzer is (raw) 1000 ppm, no error bar is shown for measurement points, which exceed this limit.

The NO_X emissions are shown in Figure 8 as a function of the turbine speed for different combustor inlet temperatures $T_{cc,in,}$ and different primary air ratios PAR.

Since NO_X is dominantly formed via the thermal path within this configuration, the NO_X emissions rise with increasing turbine speed (and therefore increasing combustion temperature). Furthermore, the curves show a slight discontinuity, which is explained by a fuel mass flow controller, which had a slight offset at particular measurement days. This led to an offset in the desired air number, hence, some emission values have higher uncertainties. However, this does not affect the general trends and their conclusions.

For a constant PAR, an increase of $T_{HTES,fluid,out}$ is compensated by a decrease in combustion temperature. This results in significantly lower NO_X emissions. Similar behavior can be achieved by increasing PAR and therefore λ.

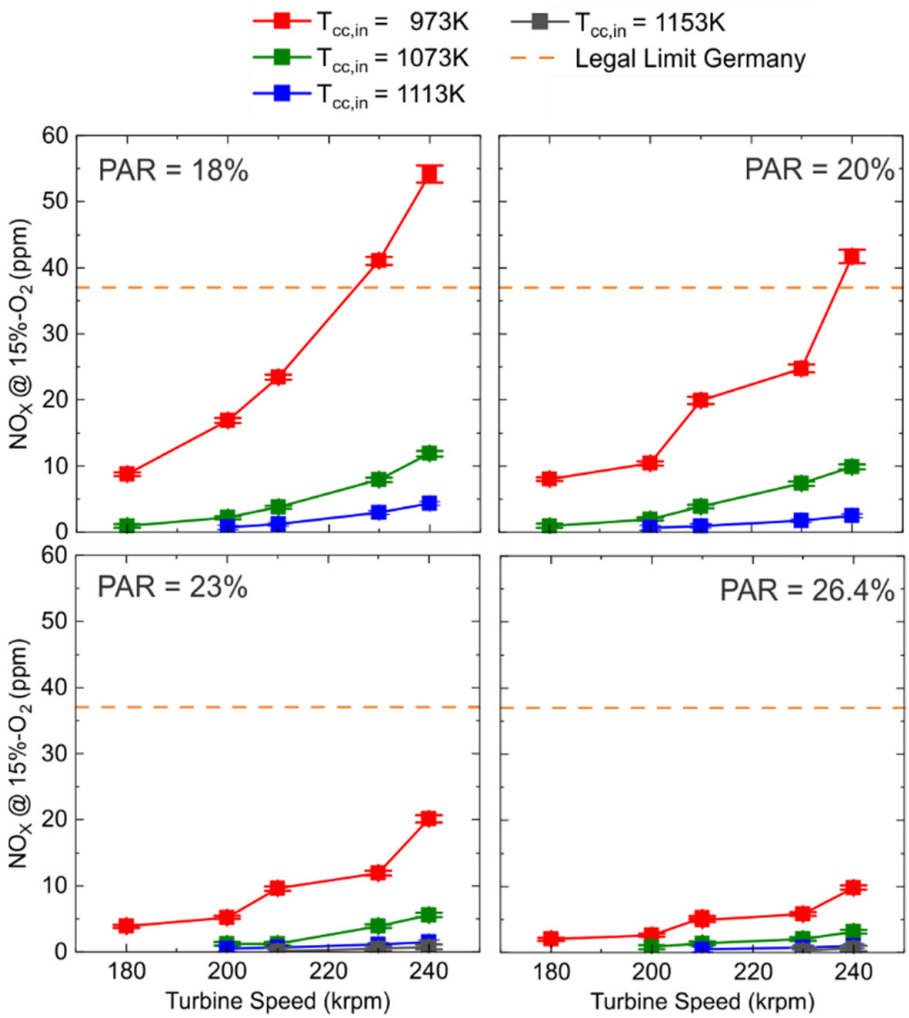

Figure 8. NO_X emissions as a function of turbine speed for different combustor inlet temperatures $T_{cc,in}$.

While the NOx emissions are low at a residual oxygen content of 15 vol% for all $T_{cc,in}$ at PAR = 23% and PAR = 26.4%, they increase for low $T_{cc,in}$ at PAR $\leq$ 20%, and exceed the German emission limit [56]. Hence, for low NO_X emissions, PAR should be as large as possible.

The shape of the CO emission curve depends on the oxygen content, as well as on the combustion temperature combined with the residence time. At high combustion temperatures, the CO emissions decrease with the decreasing turbine speed and, therefore, the air number decreases (and oxygen content increases), as can be seen for $T_{cc,in}$ = 973 K at a PAR of 20% in Figure 9. When combustion temperatures are lower, e.g., for $T_{cc,in}$ = 1113 K, the CO emissions rise with the decreasing turbine speed. Here, the rates of the chemical reactions slow down and the residence time for the CO oxidation is not sufficient anymore. For the theoretic combustion temperatures, see Figure 7. The minimum of the CO emissions at a constant primary air ratio is shifted to higher turbine speeds with increasing combustor inlet temperatures. At PAR = 20%, the legal limit in Germany of 80 ppm at a residual oxygen content of 15 vol% is exceeded at base load for $T_{cc,in}$ = 973 K [56]. For this low combustor inlet temperature, the primary air ratio should be shifted to higher values. However, when shifted to higher values, the limit is exceeded for the high combustor inlet temperatures of 1113 K and 1153 K in part load operation. Since the regulations are only valid for loads of more than 70%, which corresponds to turbine speeds of approximately 217 krpm at $T_{cc,in}$ = 973 K, at least $T_{cc,in}$ = 1113 K would be possible at PAR = 23% in terms of CO emissions as well as of NO_X emissions. In order to get low CO emissions at high

combustor inlet temperatures, PAR should be as low as possible, whereas for low inlet temperatures, it should be as high as possible.

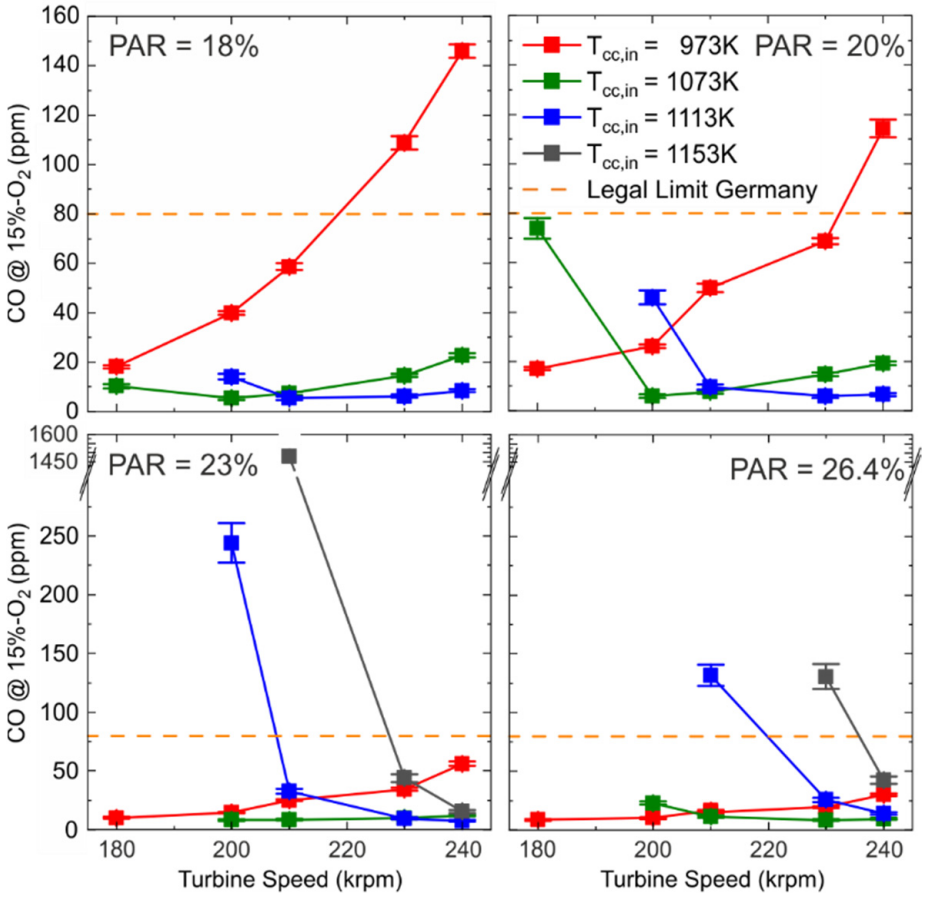

Figure 9. CO emissions as a function of turbine speed for different combustor inlet temperatures $T_{cc,in}$.

For deriving a PAR, different aspects have to be considered. With the assumption that the MGT-HTES power plant has not to be operated under cold start conditions, as the last elements of the HTES are electrically heated to preheat the air up to the combustor inlet temperature of the conventional MGT, the minimum $T_{cc,in}$ will not fall below 973 K. On the other hand, the combustor should be able to operate with a $T_{cc,in}$ as high as possible, in order to support the power production as soon as possible when $T_{HTES,fluid,out}$ declines. Furthermore, German legal limits for NO_X (37 ppm @ 15 vol% O_2) and CO (80 ppm @ 15 vol% O_2) need to be considered. Depending on the region, other legal limits may be necessary to consider. For these assumptions, a PAR of 23% seems optimal to fulfill all requirements and enable a broad operating range while achieving low emissions. At this PAR the NO_X emissions are far below the legal limit for all $T_{cc,in}$ while the CO emissions are clearly under the limit as well. At higher combustor inlet temperatures, the experimental investigations show a limited operating range. At a combustor inlet temperature of 1153 K, a minimum turbine speed of approximately 230 krpm seems feasible, since the CO emissions rise steeply at lower turbine speeds, indicating the approach to the lean stability limit. An enlargement of the operation range at high combustor inlet temperature could be achieved for example by using an adaptive dilution geometry.

5. Conclusions

In the present paper, a fundamental, application-independent potential analysis of an MGT coupled with an HTES, as well as an experimental investigation of the first combustor design for the power plant were pursued.

First, a qualitative analysis of the influence of an HTES on an MGT was presented showing that HTES has a big influence on the combustor inlet temperature and hence on the combustion process and operating range. Additionally, using an HTES at maximum temperature prevents low part load operation due to temperature limitations of the recuperator, if no mitigation strategy, like a cooling air bypass to the combustor, is integrated. For the other MGT components, no major influence was indicated.

Then, the process simulation tool was introduced, which was adapted for this study. Here, a simplified HTES model was derived and implemented, to pursue quasi-stationary simulations of the MGT-HTES-CHP.

Subsequently, the results of the numerical studies and the experimental investigation of the combustor were presented. For numerically studying the influence of HTES on MGT two different HTES models representing different commercially available, low-cost, ceramic inventory options were derived. The numerical results showed that the optimum performance gain in terms of efficiency and fuel savings for one discharge cycle of the studied cases is achieved when the HTES design is based on honeycomb bricks with high porosity and a high specific surface, as well as a sharp decline of $T_{HTES,fluid,out}$. Here, due to the stored heat 44% less fuel is needed within one discharge cycle of the HTES. Hence, if only fuel consumption is considered, the averaged electrical efficiency within the discharge process accounts for 25.8% compared to 14.8% of the stand-alone MGT while the electrical and thermal power output remains almost the same.

For investigating the impact of different $T_{HTES,fluid,out}$ on the combustor emissions and stability and to determine the optimum primary air ratio (PAR), a jet-stabilized combustor was designed and operated with air inlet temperatures ($T_{cc,in}$) of up to 1153 K and PAR of 18%, 20%, 23%, and 26.4%. The combustor could be stably operated at all $T_{cc,in}$. It should be noted that the stable operating range at high $T_{cc,in}$ was limited to higher turbine speeds since the combustion becomes too lean at part load. Besides the combustion stability, the emissions were considered when choosing the optimum PAR. For the presented case, a PAR of 23% seems to be the optimal compromise between a wide stable operating range and complying with emission limits within the HTES fluid outlet temperature range. At this PAR, the combustor meets the local (German) emission requirements for NO_X and CO emissions for $T_{HTES,fluid,out}$ from 973 to 1073 K, and even up to 1113 K if the operation is limited to high turbine speeds.

The experimental studies proved the feasibility of the developed combustor design for the application in the MGT-HTES power plant by providing operating ranges with high combustion stability and very low emissions. Moreover, it was found that the operating range can be expanded while emissions are minimized, by applying a variable geometry to control the PAR in dependence on the combustor inlet temperature. A concept for realizing a variable PAR within a jet-stabilized combustion system was developed and applied for a patent (pending).

As a next step for the overall performance of the MGT-HTES power plant, the cycle simulations should be updated considering a minimum fuel mass flow for the combustor. Furthermore, the design and benefit of an HTES strongly depend on the field of application, power demand, energy pricing fluctuations, and the associated requirements concerning discharge duration. Hence, identifying a field of application and pursuing a techno-economic analysis and a broad parameter study considering more HTES parameters such as different materials, heat capacities, heat, and pressure losses would be the next step toward commercial use. Furthermore, technically and economically feasible concepts for electrically heating the cold HTES need to be addressed—either for the case when access to electricity is available or when energy from the MGT is required.

Both aspects, the variable geometry to control PAR as well as concepts for heating an HTES up to 1300 K are pursued in a follow-up project within the DLR.

Author Contributions: Conceptualization, E.A., M.H., V.D. and P.K.; Data curation, E.A. and H.S.-O.; Formal analysis, E.A. and V.D.; Funding acquisition, E.A., M.H., V.D. and P.K.; Investigation, E.A., H.S.-O., V.D. and T.K.; Methodology, E.A., H.S.-O., M.H., V.D. and T.K.; Project administration, E.A.; Software, M.H., V.D. and T.K.; Supervision, M.H. and P.K.; Visualization, E.A. and H.S.-O.; Writing—original draft, E.A., H.S.-O. and V.D.; Writing—review & editing, H.S.-O. All authors have read and agreed to the published version of the manuscript.

Funding: This research received no external funding.

Acknowledgments: The authors would like to thank Felix Grimm for the fruitful discussions and Ingo Schmidt, as well as Jürgen Roth for the support during the measurement campaign.

Conflicts of Interest: The authors declare no conflict of interest.

Nomenclature

Greek

ε	Porosity [%]
η	Efficiency [%]
Δ	Difference
λ	Air number [-]
Π	Pressure ratio [-]
ϕ	Equivalence ratio [-]
Ψ	Reduced heat loss [-]
Λ	Reduced length [-]

Alphanumeric Variables

a_v	Specific surface [m^2/m^3]
m	Mass [kg]
$\dot{m}$	Mass flow [kg/s]
p	Pressure [Pa]
P	Power out [W]
Q	Heat capacity [Wh]
$\dot{Q}$	Heat flow [W]
L/D	Length/Diameter ratio
P_D	Reduced period duration
s	Entropy [J/K]
T	Temperature [K]
t	Time [min]
X	Volumetric fraction [mol/mol]
z*	Normalized space dimension [-]

Abbreviations

ad	Adiabatic
ave	Average
comp	Compressor
el	Electrical
in	Inlet
isen	Isentropic
ov	Overall
rec	Recuperator
st	Stoichiometric
th	Thermal
turb	Turbine
AFR	Air fuel ratio
ATM	Atmospheric (Test Rig)
CC	Combustor
CCGT	Combined-cycle gas turbines

CHP	Combined heat and power
CO	Carbon monoxide
DLR	German Aerospace Centre
HTES	High temperature energy storage
MGT	Micro gas turbine
NO_X	Nitrogen oxides
LBO	Lean blow-off
O_2	Oxygen (molecular)
PAR	Primary air ratio
TIT	Turbine inlet temperature
TOT	Turbine outlet temperature
WHX	Water heat exchanger

References

1. Bundesministerium für Umwelt, Naturschutz und Nukleare Sicherheit. Klimaschutzplan 2050 Klimaschutzpolitische Grundsätze und Ziele der Bundesregierung. Available online: https://www.bmu.de/fileadmin/Daten_BMU/Download_PDF/Klimaschutz/klimaschutzplan_2050_bf.pdf (accessed on 21 April 2020).
2. Gemmer, B. Flexible Combined Heat and Power (CHP) Systems. Available online: https://www.energy.gov/sites/prod/files/2018/01/f47/Flexible%20CHP%20Comms_01.18.18_compliant.pdf (accessed on 14 April 2020).
3. Thomas, B. *Mini-Blockheizkraftwerke: Grundlagen, Gerätetechnik, Betriebsdaten*, 2nd ed.; Vogel Buchverlag: Würzburg, Germany, 2011; ISBN 9783834332110.
4. Pilavachi, P.A. Power Generation with Gas Turbine Systems and Combined Heat and Power. *Appl. Therm. Eng.* **2000**, *20*, 1421–1429. [CrossRef]
5. Schaumann, G.; Schmitz, K.W. *Kraft-Wärme-Kopplung*; Springer: Berlin/Heidelberg, Germany, 2010; ISBN 978-3-642-01424-6.
6. Pilavachi, P.A. Mini- and micro-gas turbines for combined heat and power. *Appl. Therm. Eng.* **2002**, *22*, 2003–2014. [CrossRef]
7. Schmidt, F.W.; Willmott, A.J. *Thermal Energy Storage and Regeneration*; Hemisphere Publication Corp: Washington, DC, USA, 1981; ISBN 978-0070553460.
8. Kuravi, S.; Trahan, J.; Goswami, D.Y.; Rahman, M.M.; Stefanakos, E.K. Thermal energy storage technologies and systems for concentrating solar power plants. *Prog. Energy Combust. Sci.* **2013**, *39*, 285–319. [CrossRef]
9. Flueckiger, S.M.; Iverson, B.D.; Garimella, S.V.; Pacheco, J.E. System-level simulation of a solar power tower plant with thermocline thermal energy storage. *Appl. Energy* **2014**, *113*, 86–96. [CrossRef]
10. Powell, K.M.; Edgar, T.F. Modeling and control of a solar thermal power plant with thermal energy storage. *Chem. Eng. Sci.* **2012**, *71*, 138–145. [CrossRef]
11. Spelling, J.; Laumert, B.; Fransson, T. Advanced Hybrid Solar Tower Combined-cycle Power Plants. *Energy Procedia* **2014**, *49*, 1207–1217. [CrossRef]
12. Stahl, K.; Moser, P.; Marquardt, R.; Siebert, M.; Kessler, S.; Maier, F.; Krüger, M.; Zunft, S.; Dreißigacker, V.; Hahn, J. *Flexibilisierung von Gas- und Dampfturbinenkraftwerken durch den Einsatz von Hochtemperatur-Wärmespeichern (FleGs): F&E Vorhaben zur Vorbereitung von Hochtemperatur-Wärmespeichern und deren Integration in den Gas- und Dampfturbinenprozess; Abschlussbericht an BMWi/PTJ; Laufzeit: 01.12.2009–31.12.2012*; Technische Informationsbibliothek u. Universitätsbibliothek: Hannover, Germany, 2013. [CrossRef]
13. Li, D.; Hu, Y.; Li, D.; Wang, J. Combined-cycle gas turbine power plant integration with cascaded latent heat thermal storage for fast dynamic responses. *Energy Convers. Manag.* **2019**, *183*, 1–13. [CrossRef]
14. Li, D.; Wang, J. Study of supercritical power plant integration with high temperature thermal energy storage for flexible operation. *J. Energy Storage* **2018**, *20*, 140–152. [CrossRef]
15. Wojcik, J.; Wang, J. Technical Feasibility Study of Thermal Energy Storage Integration into the Conventional Power Plant Cycle. *Energies* **2017**, *10*, 205. [CrossRef]
16. Gkoutzamanis, V.; Chatziangelidou, A.; Efstathiadis, T.; Kalfas, A.; Traverso, A.; Chiu, J. Thermal Energy Storage For Gas Turbine Power Augmentation. *J. Glob. Power Propuls. Soc.* **2019**, *3*, 592–608. [CrossRef]
17. Bédécarrats, J.-P.; Strub, F. Gas turbine performance increase using an air cooler with a phase change energy storage. *Appl. Therm. Eng.* **2009**, *29*, 1166–1172. [CrossRef]
18. Amelio, M.; Morrone, P. Numerical evaluation of the energetic performances of structured and random packed beds in regenerative thermal oxidizers. *Appl. Therm. Eng.* **2007**, *27*, 762–770. [CrossRef]
19. Dreißigacker, V.; Belik, S. System Configurations and Operational Concepts for Highly Efficient Utilization of Power-to-Heat in A-CAES. *Appl. Sci.* **2019**, *9*, 1317. [CrossRef]
20. Krüger, M.; Muslubas, S.; Loeper, T.; Klasing, F.; Knödler, P.; Mielke, C. Potentials of Thermal Energy Storage Integrated into Steam Power Plants. *Energies* **2020**, *13*, 2226. [CrossRef]
21. Fricker, H.W. Regenerative thermal storage in atmospheric air system solar power plants. *Energy* **2004**, *29*, 871–881. [CrossRef]
22. Pacheco, J.E.; Showalter, S.K.; Kolb, W.J. Development of a Molten-Salt Thermocline Thermal Storage System for Parabolic Trough Plants. *J. Sol. Energy Eng.* **2002**, *124*, 153–159. [CrossRef]

23. Tamme, R.; Laing, D.; Steinmann, W.-D. Advanced Thermal Energy Storage Technology for Parabolic Trough. *J. Sol. Energy Eng.* **2004**, *126*, 794–800. [CrossRef]
24. Steinmann, W.-D.; Tamme, R. Latent Heat Storage for Solar Steam Systems. In Proceedings of the 13th Solar-PACES International Symposium on Concentrated Solar Power and Chemical Energy Technology, Sevilla, Spain, 20–23 June 2006.
25. Kölbig, M.; Bürger, I.; Linder, M. Thermal applications in vehicles using Hydralloy C5 in single and coupled metal hydride systems. *Appl. Energy* **2021**, *287*, 116534. [CrossRef]
26. Linder, M.; Utz, I.; Schaube, F.; Molenda, M.; Wörner, A. Gas-Solid Reactions for Heat Applications. In Proceedings of the 5th International Hydrogen & Energy Symposium, Stoos, Switzerland, 23–28 January 2011; p. 21.
27. Dreißigacker, V. Thermal Battery for Electric Vehicles: High-Temperature Heating System for Solid Media Based Thermal Energy Storages. *Appl. Sci.* **2021**, *11*, 10500. [CrossRef]
28. Belik, S.; Dreißigacker, V. Electro-Thermal Analysis of Inductively Heated and Aerated Rod Bundle for Adiabatic Compressed Air Energy Storage. In Proceedings of the 12th International Renewable Energy Storage Conference, Düsseldorf, Germany, 13–15 March 2018.
29. Wünning, J.A.; Wünning, J.G. Flameless Oxidation to Reduce Thermal NO-Formation. *Prog. Energy Combust. Sci.* **1997**, *23*, 81–94. [CrossRef]
30. Cavaliere, A.; De Joannon, M. Mild Combustion. *Prog. Energy Combust. Sci.* **2004**, *30*, 329–366. [CrossRef]
31. Zornek, T.; Monz, T.; Aigner, M. Experimentelle Charakterisierung eines Holzgas-Brenners für Mikrogasturbinen. In Proceedings of the VDI, 26th German Flame Day–Combustion and Furnaces, Duisburg, Deutschland, 11–12 September 2013; Volume 2161, pp. 775–778.
32. Zornek, T.; Monz, T.; Aigner, M. A Micro Gas Turbine Combustor for the use of Product Gases from Biomass Gasification. In Proceedings of the 6th European Combustion Meeting, ECM 2013, Lund, Sweden, 25–28 June 2013; ISBN 978-91-637-2151-9.
33. Zornek, T.; Monz, T.; Aigner, M. Effizient, flexibel, sauber-Flox-Brennkammersysteme für Mikrogasturbinen. *BWK* **2014**, *66*, 13–16.
34. Bower, H.E.; Grimm, F.; Schwärzle, A.; Roth, J.; Zornek, T.; Kutne, P. Experimental Analysis of the Fuel Flexibility of a Jet-Stabilized Micro Gas Turbine Combustor Designed for Low Calorific Gases. In Proceedings of the GPPS Forum 2018, GPPS-2018, Zurich, Switzerland, 10–12 January 2018.
35. Zanger, J.; Monz, T.; Aigner, M. Experimental Investigation of the Influence of Combustor Cooling on the Characteristics of a FLOX-Based Micro Gas Turbine Combustor. In *Progress in Gas Turbine Performance*; Benini, E., Ed.; InTech: London, UK, 2013; pp. 165–184, ISBN 978-953-51-1166-5.
36. Zanger, J.; Monz, T.; Aigner, M. Experimental Investigation of the Combustion Characteristics of a Double-Staged FLOX-Based Combustor on an Atmospheric and a Micro Gas Turbine Test Rig. In Proceedings of the ASME Turbo Expo: Turbine Technical Conference and Exposition-2015, Montreal, QC, Canada, 15–19 June 2015; ASME: New York, NY, USA, 2015, ISBN 978-0-7918-5662-8.
37. Seliger-Ost, H.; Kutne, P.; Zanger, J.; Aigner, M. Experimental Investigation of the Impact of Biogas on a 3 kW Micro Gas Turbine FLOX®-Based Combustor. *J. Eng. Gas Turbines Power* **2021**, *143*, 081020. [CrossRef]
38. Lingstädt, T.; Grimm, F.; Krummrein, T.; Bücheler, S.; Aigner, M. Experimental Investigation Of An SOFC Off-Gas Combustor For Hybrid Power Plant Usage With Low Heating Values Realised by Natural Gas Addition. In Proceedings of the GPPS Forum 2018, GPPS-2018, Zurich, Switzerland, 10–12 January 2018.
39. Seliger, H.; Huber, A.; Aigner, M. Experimental Investigation of a FLOX-Based Combustor For a Small-Scale Gas Turbine Based CHP System Under Atmospheric Conditions. In Proceedings of the ASME Turbo Expo: Turbine Technical Conference and Exposition-2015, Montreal, QC, Canada, 15–19 June 2015; ASME: New York, NY, USA, 2015, ISBN 978-0-7918-5662-8.
40. Hasemann, S.; Seliger, H.; Kutne, P.; Aigner, M. Experimental and Numerical Design Study for a Small Scale Jet-Stabilized Micro Gas Turbine Combustor. In Proceedings of the ASME Turbo Expo: Turbomachinery Technical Conference and Exposition-2018, Oslo, Norway, 11–15 June 2018; American Society of Mechanical Engineers: New York, NY, USA, 2018, ISBN 978-0-7918-5098-5.
41. Lingstädt, T.; Grimm, F.; Krummrein, T.; Kutne, P.; Aigner, M. Atmospheric Experimental Investigations of a Jet-Stabilized SOFC Off-Gas Combustor for a Hybrid Power Plant operated with Biogas. In Proceedings of the AIAA Scitech 2019 Forum, San Diego, CA, USA, 7–11 January 2019.
42. Bücheler, S.; Huber, A.; Aigner, M. Development of a Jet-Stabilized Combustion System for the Use of Low-Caloric SOFC Off-Gas. In Proceedings of the ASME Turbo Expo: Turbine Technical Conference and Exposition-2017, Charlotte, NC, USA, 26–30 June 2017; The American Society of Mechanical Engineers: New York, NY, USA, 2017, ISBN 978-0-7918-5077-0.
43. Panne, T.; Widenhorn, A.; Boyde, J.; Matha, D.; Abel, V.; Aigner, M. Thermodynamic Process Analyses of SOFC/GT Hybrid Cycles. *AIAA J.* **2007**, *1*, 25–27.
44. Henke, M.; Monz, T.; Aigner, M. Inverted Brayton Cycle with exhaust gas recirculation-a numerical investigation. *J. Eng. Gas Turbines Power* **2013**, *135*, 091203. [CrossRef]
45. Krummrein, T.; Henke, M.; Kutne, P. A highly flexible approach on the steady-state analysis of innovative micro gas turbine cycles. In Proceedings of the ASME Turbo Expo: Turbomachinery Technical Conference and Exposition-2018, Oslo, Norway, 11–15 June 2018; American Society of Mechanical Engineers: New York, NY, USA, 2018, ISBN 978-0-7918-5098-5.

46. Agelidou, E.; Monz, T.; Huber, A.; Aigner, M. Experimental Investigation Of An Inverted Brayton Cycle Micro Gas Turbine For CHP Application. In Proceedings of the ASME Turbo Expo: Turbine Technical Conference and Exposition-2017, Charlotte, NC, USA, 26–30 June 2017; The American Society of Mechanical Engineers: New York, NY, USA, 2017, ISBN 978-0-7918-5077-0.
47. Krummrein, T.; Henke, M.; Kutne, P.; Aigner, M. Numerical analysis of operating range and SOFC-off-gas combustor requirements of a biogas powered SOFC-MGT hybrid power plant. *Appl. Energy* **2018**, *232*, 598–606. [CrossRef]
48. Goos, E.; Burcat, A.; Rustic, B. Extended Third Millennium Ideal Gas and Condensed Phase Thermochemical Database for Combustion with Updates from Active Thermochemical Tables. Available online: http://atct.anl.gov/ (accessed on 12 March 2020).
49. Henke, M.; Monz, T.; Aigner, M. Validation of a t100 micro gas turbine steady-state simulation tool. In Proceedings of the ASME Turbo Expo: Turbine Technical Conference and Exposition-2015, Montreal, QC, Canada, 15–19 June 2015; ASME: New York, NY, USA, 2015, ISBN 978-0-7918-5662-8.
50. Micro Turbine Technology, b.v. The Core of the EnerTwin. Available online: https://www.enertwin.com/enertwin-en/the-enertwin (accessed on 14 April 2020).
51. Visser, W.; Oostveen, M. Development of a 3kW micro turbine for CHP applications. In Proceedings of the ASME Turbo Expo 2010, Glasgow, UK, 14–18 June 2010; ASME: New York, NY, USA, 2010, ISBN 978-0-7918-4396-3.
52. Visser WP, J.; Shakariyants, S.A.; De Later MT, L.; Haj Ayed, A.; Kusterer, K. Performance Optimization of a 3kW Microturbine for CHP Applications. In Proceedings of the ASME Turbo Expo 2012, Presented at the 2012 ASME Turbo Expo, Copenhagen, Denmark, 11–15 June 2012; ASME: New York, NY, USA, 2012, ISBN 978-0-7918-4467-0.
53. Ismail, K.; Stuginsky, R., Jr. A parametric study on possible fixed bed models for pcm and sensible heat storage. *Appl. Therm. Eng.* **1999**, *19*, 757–788. [CrossRef]
54. Hausen, H. *Wärmeübertragung im Gegenstrom, Gleichstrom und Kreuzstrom*; Springer: Berlin/Heidelberg, Germany, 1950; ISBN 978-3-642-53135-4.
55. Schmidt, I. Experimentelle Untersuchung Eines FLOX®-Basierten Brenners für Eine Mikrogasturbine mit Hohen Brennereintrittstemperaturen. Master's Thesis, Universität Stuttgart, Stuttgart, Germany, 2021.
56. Bundesministerium für Umwelt, Naturschutz und nukleare Sicherheit. Neufassung der Ersten Allgemeinen Verwaltungsvorschrift zum Bundes-Immisionsschutzgesetz (Technische Anleitung zur Reinhaltung der Luft–TA Luft). Available online: https://umweltmessung.com/wp-content/uploads/TA-Luft-2021-1.pdf (accessed on 25 January 2022).